CHAPTER 4

GROWTH OF SILICON NANOWIRES ON ITO COATED GLASS USING AURUM CATALYST

4.1 INTRODUCTION

In this chapter, the role of In in the ITO-coated glass substrate on the growth of SiNWs using Au catalyst was studied. In the first part of this work, SiNWs were prepared by evaporation of Au followed by dissociation of SiH_4 and H_2 gas using rf-PECVD onto c-Si and ITO-coated glass substrates (Set 1). The evaporated Au in H_2 plasma formed islands of Au on the c-Si, which acted as a catalyst to induce the growth of SiNWs, while for the ITO-coated glass substrate, the In/Au alloy catalyst islands were formed by abstraction of In from ITO using H_2 plasma treatment combined with evaporation of Au wire placed on the heated tungsten filament in the deposition system. A comparative study on the catalytic growth of SiNWs using Au and In/Au catalyst on c-Si and ITO-coated glass respectively was done. In the second part of this work, SiNWs were grown by simultaneous evaporation of Au and dissociation of SiH_4 and H_2 on H_2 plasma treated ITO-coated glass (Set 2). In this case, the heated tungsten filament played a double role of evaporating Au wire and dissociating SiH_4 and H_2 gases simultaneously, while the dissociation of the gases was assisted by rf plasma discharge to enhance the hot-wire assisted PECVD system. The effects of rf power on growth and structural properties of the as-grown SiNWs were investigated.

4.2 SILICON NANOWIRES GROWN USING AURUM CATALYST ON CRYSTAL SILICON AND ITO GLASS

4.2.1 Catalyst islands formation on c-Si and ITO-coated glass

4.2.1 a) Morphology and chemical composition

Figures 4.1 (a), (b) and (c) show the FESEM images of the plain ITO on glass, H_2 plasma-treated ITO-coated glass and Au evaporated on ITO-coated glass in H_2 plasma environment. H_2 plasma treatment results in the islands formation on the surface of the substrate. The FESEM image of the ITO-coated glass after 5 minutes of H_2 plasma treatment [Figure 4.1 (b)] clearly shows scattered islands with sizes varying from a few tens to 300 nm, which are sputtered out from the ITO surface. EDX scanned on those islands [Figure 4.1 (e)] shows the presence of In and typical elements of glass substrate. Thus, this indicates that the islands consist mainly of In element. The evaporation of Au onto the H_2 plasma treated ITO-coated glass may result in the diffusion of Au atoms into the In droplets. FESEM image of the ITO-coated glass after Au evaporation in H_2 plasma treatment for 5 minutes [Figure 4.1 (c)] shows a denser island distribution with sizes varying from 50 to 250 nm and the average size is ~69 ± 12 nm. The EDX scanned on those islands [Figure 4.1 (f)] shows the presence of Au and In elements, which confirms that the islands are formed from In and Au elements. The FESEM image of Au islands formed on the c-Si substrate via evaporation of the Au wire in a H_2 plasma environment is shown in Figure 4.1 (d). The sizes of Au islands vary from 24 to 60 nm and the average size is estimated to be about 38 ± 12 nm. The catalyst islands formed on c-Si mainly consist of Au element confirming that the In elements have been sputtered from the ITO-coated glass substrate.

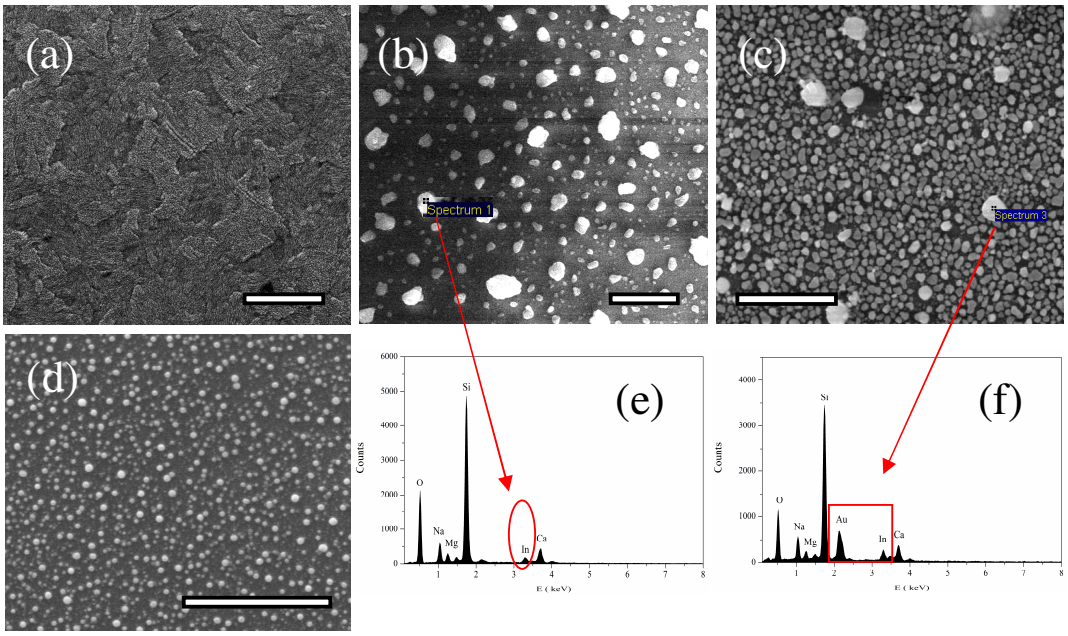

Figure 4.1: FESEM images of the ITO-coated glass substrate (a) before, (b) after 5 minutes of H_2 plasma treatment, and (c) after Au evaporation in H_2 plasma environment for 5 minutes. (Scale bar = 1 µm). (d) FESEM image of the Au evaporated in H_2 plasma on a p-type c-Si(111) substrate (e) and (f) EDX spectra taken from the catalyst islands formed in samples (b) and (c) respectively.

4.2.1 b) X-ray diffraction

XRD patterns of the ITO, H_2 plasma treated ITO, Au evaporation in H_2 plasma treatment on ITO-coated glass and p-type c-Si(111) substrates are displayed in Figure 4.2 (a) – (d), respectively. The XRD pattern of the ITO-coated glass after 5 min of H_2 plasma treatment presents a total suppression of ITO peak and the emergence of In crystalline peak. This again confirms that the extraction of In elements from ITO layer during the H_2 plasma treatment. The XRD pattern of the Au evaporated onto the ITO-coated glass substrate in H_2 plasma environment reveals the presence of Au crystalline peak as well as In(101) crystalline plane. The other In related peaks are suppressed by the incorporation of Au in the In islands. On the other hand, the XRD pattern of the Au evaporated on c-Si substrate shows the presence of only Au crystalline peaks.

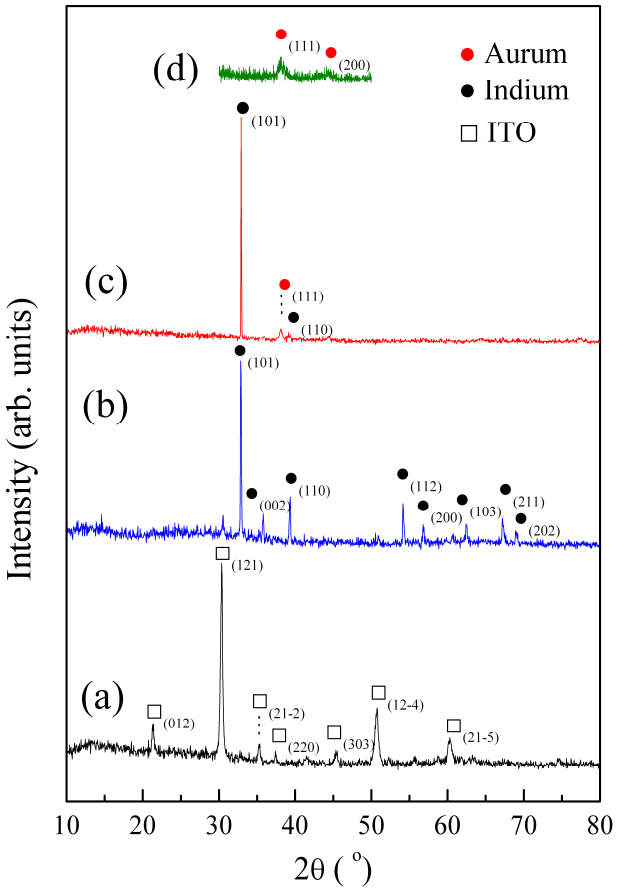

Figure 4.2: XRD patterns of the ITO-coated glass substrate (a) before, (b) after 5 minutes of H_2 plasma treatment and (c) after Au evaporation in H_2 plasma environment for 5 minutes. (d) XRD pattern of Au evaporated on p-type c-Si(111) in H_2 plasma environment for 5 minutes. The crystal plane of ITO, In and Au are indexed according to JCP2:01-088-0773, JCP2:01-085-1409 and JCP2:00-001-1174, respectively.

4.2.2 Growth of Si nanowires on c-Si and ITO-coated glass

4.2.2 a) Morphology

FESEM image of SiNWs synthesized on c-Si and ITO-coated glass substrates are presented in Figures 4.3 (a) and (b), respectively. The SiNWs grown on c-Si are relatively short in length (~870 ± 160 nm) with diameter of ~420 ± 60 nm. The NWs are mostly capped with catalyst droplets. In contrast, few microns length of SiNWs with diameter varying from 130 to 260 nm is grown on ITO-coated glass. The SiNWs are grown in random direction and are capped with large catalyst droplets.

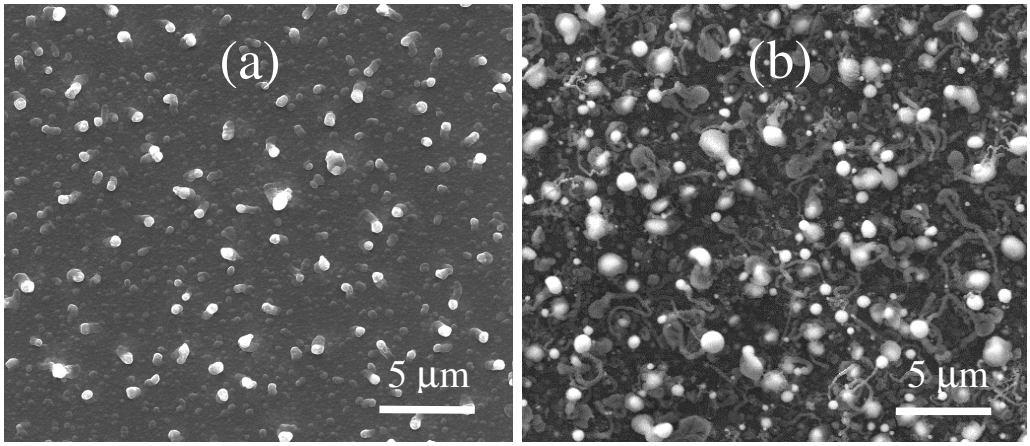

Figure 4.3: FESEM images of the SiNWs synthesized on (a) c-Si and (b) ITO-coated glass substrates.

4.2.2 b) Variation of catalyst sizes with nanowires diameters

A significant difference in catalyst size to NWs diameter ratio, $r_{c\text{-}nw}$ is observed between the Au-catalyzed and In/Au-catalyzed SiNWs. The variation of catalyst size with NWs diameter ratio for both Au- and In/Au-catalyzed SiNWs is plotted in Figure 4.4. For Au-catalyzed SiNWs, the $r_{c\text{-}nw}$ of ~1.2 obtained is consistent with values reported by others (*Salem et al. 2009; Xu et al. 2010*). The $r_{c\text{-}nw}$ for In/Au-catalyzed SiNWs of ~4.1 is relatively high compared to Au-catalyzed SiNWs. The formation of large droplets capping SiNWs is a typical phenomenon occurring in low surface tension catalyst, such as In (*Alet et al. 2008; Bettge et al. 2009; Yu et al. 2009*), Sn (*Yu et al. 2009; Yu et al. 2011*) and Ga (*Jeon et al. 2008*) induced SiNWs. The diameter mismatch between catalyst droplets and NWs is due to the low wettability of the molten In droplets which will be discussed later.

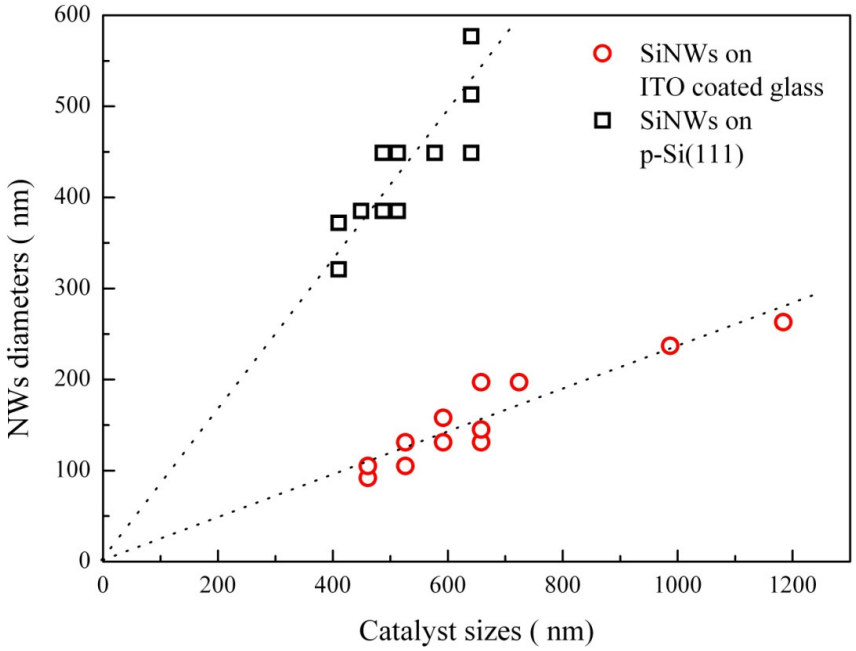

Figure 4.4: Variation of catalyst size with NWs diameter for Au-catalyzed SiNWs on p-Si(111) and In/Au-catalyzed SiNWs on ITO-coated glass.

4.2.2 c) Energy dispersion X-ray analysis

The elemental composition of the catalyst droplets and SiNWs is confirmed by EDX analysis. The EDX spectra taken on catalyst droplets and stem of the SiNWs synthesized on c-Si is shown in Figures 4.5 (a) and (b), respectively. Figures 4.5 (c) and (d) on the other hand show the EDX spectra taken on the catalyst droplets and stem of the SiNWs grown on ITO-coated glass substrate. Two peaks are observed in the EDX spectrum in Figure 4.5 (a), a strong peak formed by Si signal and a small rather broad peak produced by Au signal. Figure 4.5 (b) shows only a strong sharp peak produced by Si signal and minute signal of Au. The Si signal may partially be contributed by Si atoms in the substrate but the dominant Si signal presence in the stem of the NWs shows that the SiNWs are formed. Au/Si droplets acted as catalyst in the NWs formation. Trace of Au found in the NWs stem might due to the diffusion of Au into the NWs during the growth process (*Kawashima et al. 2007; Madras et al. 2010*). In Figures 4.5 (c) and (d), Si, Au, In, Sn and O signals are observed in the catalyst droplets,

while Si, In, Sn and O signals are observed in the stem of the NWs. The In, Sn and O signals may be contributed by the ITO layer coated glass substrate. However, the In peak is significantly higher in the EDX spectrum of the catalyst droplets compared to the stem of NWs. Moreover, Au signal observed in the catalyst droplet is absent in the stem of the NWs. This indicates that the catalyst droplets are mainly composed by In and Au elements. The In/Au alloy catalyst islands induce the growth of SiNWs, thus forming In/Au droplets capped SiNWs.

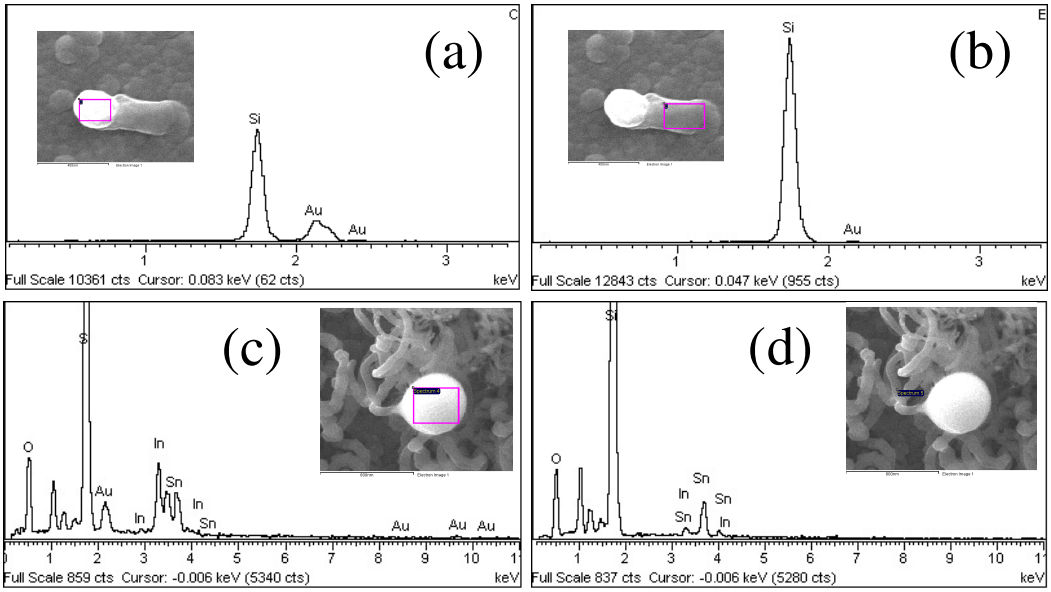

Figure 4.5: EDX spectra taken on the (a, c) catalyst droplet and (b, d) NW stem for the SiNWs grown on p-Si(111) and on ITO-coated glass, respectively.

4.2.2 d) Auger electron spectra

To further identify the composition of the In/Au-catalytic growth SiNWs, Auger electron measurement was carried out. The Auger electron spectra taken on the NWs stem, catalyst droplets and film sides using Auger microprobe are shown in Figure 4.6. The Sn, In, O and Si KLL Auger peaks located at 351 eV, 409 eV and 1557 to 1614 eV, respectively are well indexed in the figure. The Auger spectrum (a) shows significant presence of Si and O element and traces of In and Sn (relative concentration of 1.2 and 2.3%, respectively) detected within the NWs stem. From Auger spectrum (b), the

catalyst droplet reveals high signal of In (relative concentration of 6.8%) and O and weak signal of Sn, while the Si KLL peak is significantly reduced within the catalyst droplets. This strongly indicates that the catalyst droplets mainly consisted of In element. The Auger signal examined at the film component of the sample shows similar elemental composition as the NWs stem, with traces of In and Sn elements. These suggest that when SiH_x radicals are diffused into large catalyst islands, saturation of Si atoms in these islands failed to occur, therefore films were formed. However, when these radicals were diffused into smaller catalyst islands, NWs were formed. As the penetration of Auger electron measurement is < 5 nm (*Ecke et al. 2007*), most of the signals were actually obtained from the topmost layer of samples. The high signal of O detected from Auger suggests post-oxidation of dangling bonds form an oxide layer on both the catalyst droplet and stem of the NWs.

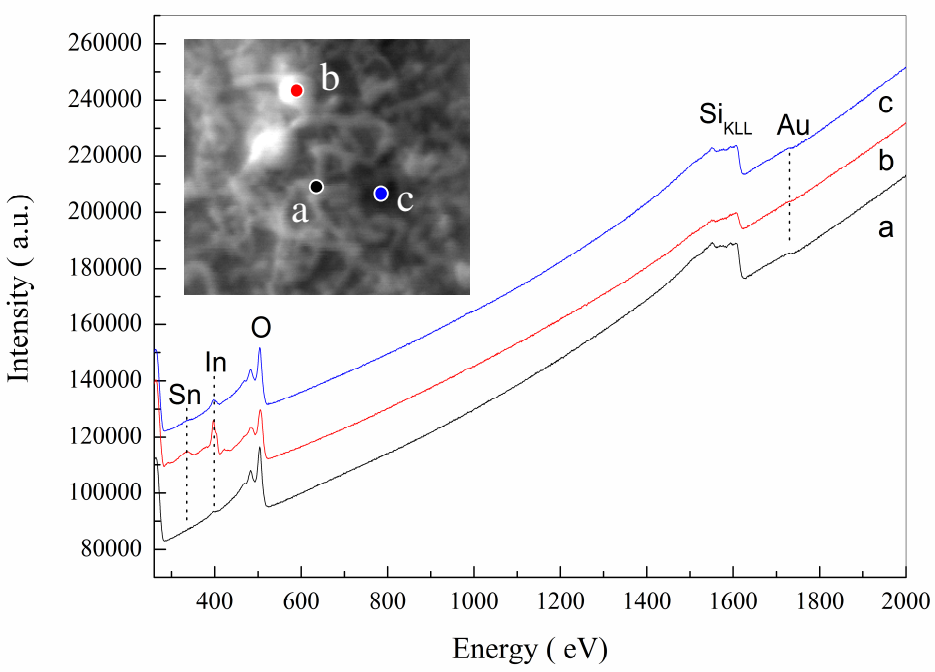

Figure 4.6: AES spectra of scanned on the (a) stem of NW, (b) catalyst droplet, and (c) film component of the samples prepared on ITO-coated glass.

4.2.2 e) X-ray diffraction

The crystallinity of the Au-catalyzed and In/Au-catalyzed SiNWs prepared on c-Si and

ITO-coated glass substrates, respectively, are shown in the XRD patterns as displayed in Figure 4.7. Si diffraction peak located at 28.4 ^{o} corresponding to (111) orientation can be observed for both samples, which confirmed the crystalline structures of SiNWs. XRD pattern of a c-Si(111) substrate [inset in Figure 4.7] reveals only Si diffraction peak at 57.6 ^{o} corresponding to (311) orientation. Thus, the Si(111) peak is only originated from the samples. Au-catalyzed SiNWs grown on c-Si substrate revealed stronger crystalline Si peak compared to the In/Au-catalyzed SiNWs grown on ITO-coated glass. The higher crystallinity of the Au-catalyzed SiNWs could be inherited from the crystalline structure from c-Si.

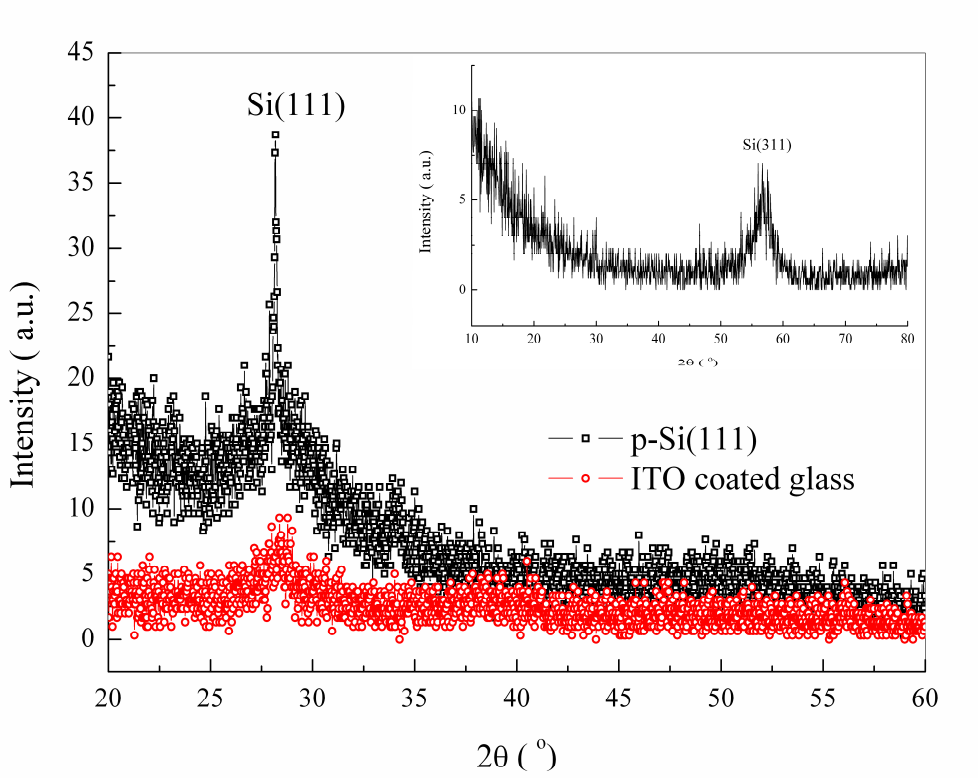

Figure 4.7: XRD patterns of the SiNWs prepared on c-Si(111) and ITO-coated glass substrates. Inset in the figure is the XRD pattern of a p-type c-Si(111) substrate.

4.3 SILICON NANOWIRES GROWN BY SIMULTANEOUS AURUM EVAPORATION AND SOURCE GAS DECOMPOSITION USING HOT-WIRE ASSISTED PLASMA ENHANCED CHEMICAL VAPOUR DEPOSITION: EFFECT OF RF POWER

From the results in section 4.2, the SiNWs formed on ITO-coated glass substrate were relatively longer in length compared to the SiNWs on c-Si substrates although synthesized under same conditions. The morphology also showed the formation of a large catalyst droplet capping on NWs and the catalyst directed growth in random direction. Therefore, the studies on the synthesis and characteristics of the SiNWs on ITO-coated glass substrate are carried out in the following section. In this part of the work, Au wire was evaporated simultaneously with the dissociation of SiH_4 and H_2 gases. The Au wire was evaporated by the heated tungsten filament while the SiH_4 and H_2 gases were dissociated by the hot filament as well as plasma discharge. The effect of rf power on the growth and structural properties of the grown SiNWs were investigated.

4.3.1 Formation of Si nanowires and microstructures

4.3.1 a) Morphology

Figures 4.8 (a) – (e) show the FESEM images of samples prepared on ITO-coated glass at different rf powers. The morphologies of the as-synthesized SiNWs were found to be significantly influenced by the applied rf power. For the sample prepared at rf power of 20 W, two types of NWs were observed on the substrate [Figure 4.9 (a)]. Winded wires with diameters of ~300 nm and lengths of ~5 μm extend from catalyst droplets of 500 to 1,000 nm in diameter and spiral NWs with diameters of ~60 nm induced by the smaller catalyst droplets were present on the substrate. Laterally grown NWs with diameters of few tens nanometers from the NWs stem with large catalyst droplets were also observed. These NWs are similar to the Ga-catalyzed SiNWs observed by Jeon et al. (*Jeon et al.*

2008). SiNWs with lengths of a few microns grown at rf power of 40 W showed more uniform diameter of ~100 nm [Figure 4.9 (b)]. The number of catalyst droplets on the surface was also reduced. NWs without catalyst droplets on top were dispersed randomly on the substrate. The diameters of SiNWs significantly increased to ~180 nm for the sample prepared at 60 W [Figure 4.9 (c)]. The synthesized NWs were shorter in length, originally tens of nanometers but are reduced to ~4 μm when deposited at that rf power. Catalyst droplets free NWs were more dominant on the substrate. High density of SiNWs was formed in the sample prepared at rf power of 80 W [Figure 4.9 (d)]. The diameters of NWs ranged from 60 to 400 nm and the lengths extended to a few tens of microns. Most of the NWs were capped by catalyst droplets on the tips. At rf power of 100 W (power density ~1273 $mWcm^{-2}$), the growth of SiNWs was totally suppressed where only micron size spherical structures were formed [Figure 4.9 (e)]. They were uniformly distributed on the surface of the substrate. The diameters of the spherical microstructures varied from 400 to 1,000 nm. The suppression of SiNWs growth might be due to the deactivation of catalyst resulting from the high rf power discharge of H_2 diluted SiH_4. Similar results were reported by Liu group on studying of the effects of rf power on the growth of carbon nanostructures (*Liu et al. 2010*).

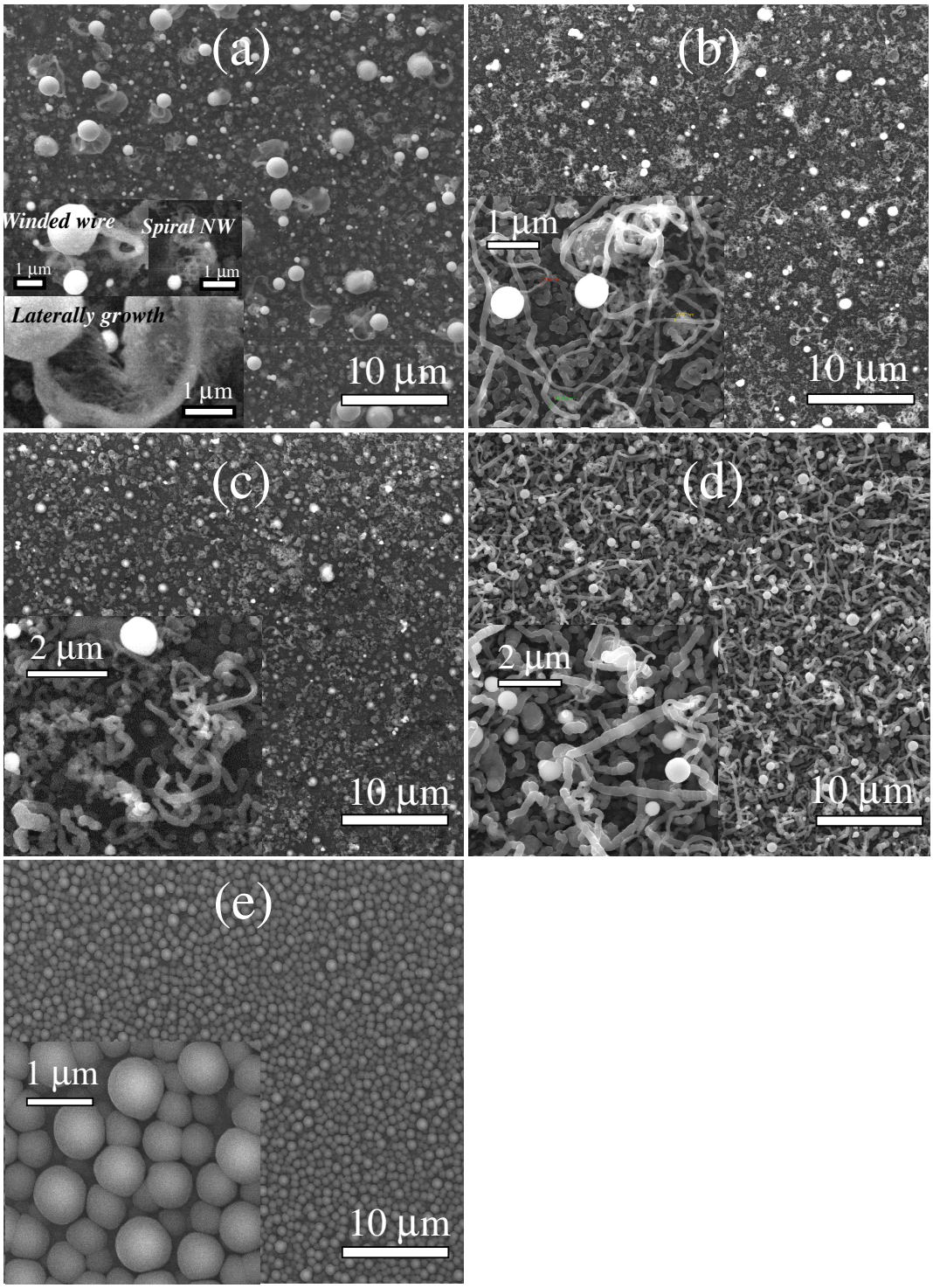

Figure 4.8: FESEM images of the SiNWs and microstructures prepared at different rf power of (a) 20 W, (b) 40 W, (c) 60 W, (d) 80 W, and (e) 100 W for 30 minutes deposition. Inset is the high magnification FESEM images of the respective samples.

4.3.1 b) Variation of diameters distribution and number density of the nanowires with rf power

A quantitative study of the diameter distribution of SiNWs was performed by measuring diameter from FESEM images and is shown in Figure 4.9. The analysis shows that the diameters of SiNWs increased with the increase of rf power. For samples prepared at rf power of 20 W, two types of wired structures are formed, i.e. winded wires with diameters ranging from 300 to 400 nm (average value of 358 nm) and spiral NWs in diameters ranging from 20 to 160 nm (average value of 70 nm) respectively. For the sample prepared at rf power of 40 and 60 W, the diameters of NWs ranged from 40 to 180 nm and 40 to 220 nm, respectively. The average values of NWs diameters increased from 97 to 113 nm for the samples prepared at 40 to 60 W. When the rf power is increased to 80 W, the diameter ranges became wider (60 to 400 nm). They are categorized into three regions: NWs with diameters of less than 200 nm; between 200 and 300 nm, larger than 300 nm. The corresponding average values of NWs diameters were calculated as 128, 233 and 340 nm, respectively. Furthermore, the number density of SiNWs increased from ~0.4 μm^{-2} (20 W) to ~0.9 μm^{-2} (80 W) as shown in the inset of Figure 4.9. It showed that the increase in rf power can actually increase the yield of SiNWs when synthesized by this technique provided the critical power density is not exceeded.

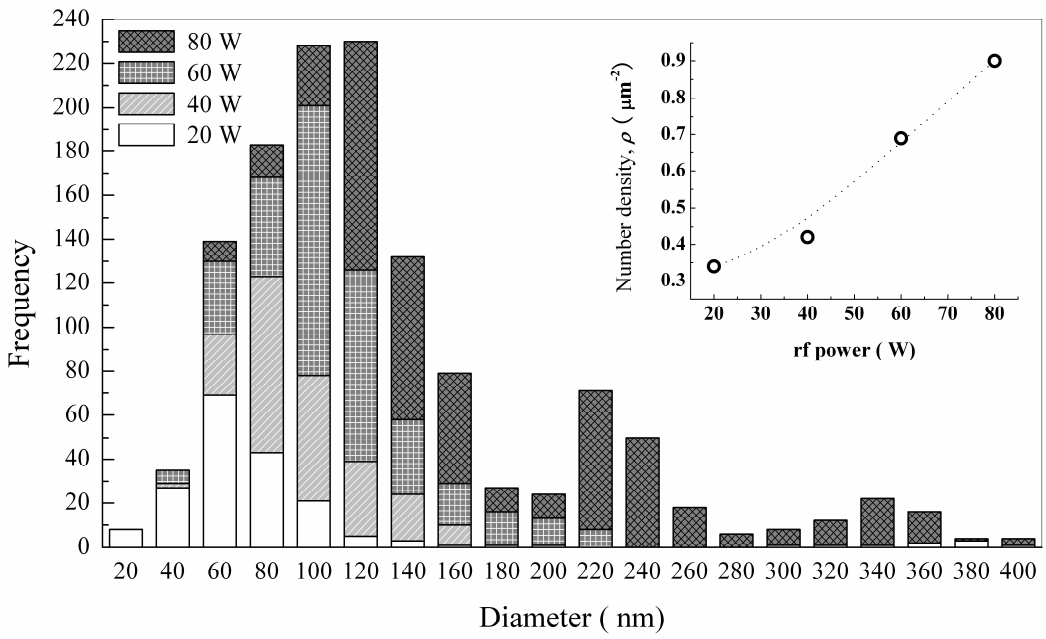

Figure 4.9: Diameter distributions of SiNWs synthesized at different rf power of 20, 40, 60 and 80 W. Inset is the variation of number density, ρ, of SiNWs with rf power.

4.3.1 c) Discussion

Increase in rf power is capable of increasing plasma ion bombardment on the growth surface and increasing primary dissociation of SiH_4 molecules. In the plasma sheath, the substrates are bombarded by ionic species with kinetic energy of several tens of eV (*Surendra and Graves 1991b*). Ion energy (E_{ion}) is qualitatively related to the sheath voltage (V) and gas pressure (P) as:

$$E_{ion} \propto V^{\frac{4}{5}} P^{-\frac{1}{2}} \tag{4.1}$$

where the sheath voltage is directly proportional to input plasma power (*Lim et al. 2010*). In the vacuum reactor, the gas flow rate and pressure are fixed. Hence, increase in rf power is expected to generate higher kinetic energy ions, which randomly bombard the growth surface. The ion bombardments could result in breaking up the large catalyst droplets on the growth surface into smaller droplets. This would increase the surface to volume ratio of the droplets and enhance the diffusion rate of the energetic SiH_x species into these smaller droplets. The Si atoms in the droplets would saturate at a faster rate

and the supersaturate Si atoms would be phased and separated out at a higher rate to form SiNWs. However, the surface of the NWs exposed to the SiH_x species in the plasma sheath could result in a sidewall deposition. This would increase the diameter of the NWs for high rf power deposition. At rf power of 80 W, the high density of the NWs is confined in a crowded area which reduces the inter-NWs spaces. Therefore, the only area which is exposed to the plasma will have substantial growth and it causes the formation of non-uniform diameters in SiNWs.

The increase in rf power may also influence the chemical composition of the ionic species in the plasma. In PECVD, primary dissociation of SiH_4 molecules is expressed by the following reactions:

$$e + SiH_4 \rightarrow nH + SiH_{4-n} \tag{4.2}$$

where n=1, 2, 3 which depends on the energy of electron. The threshold energy (8.75 eV) for SiH_3 generation is the lowest compared to SiH_2 and SiH (*Perrin et al. 1996*). Secondary gas-phase reactions occur when the SiH_x species react with the SiH_4 parent molecules to form more complex silane species (Si_xH_y). This reaction usually involves short lifetime species of SiH_2 and SiH rather than SiH_3 (*Kondo et al. 2003*). Increase in rf power results in an increase in primary dissociation and limits the secondary reaction. This reduces the formation of SiH_3 species in the plasma and thus reduces the formation of nucleation sites for Si film growth due to the abstraction of Si-H bonds and the growth of ordered Si:H film as a result of diffusion of SiH_3 radicals into these growth sites. Increase in rf power also increases dissociation of the H_2 gas resulting in an increase in reactive H atoms for H etching effects which also creates nucleation sites for ordered film growth. The increase in SiH_x species as a result of increase in rf power increases the size and yield of SiNWs in the film as these species are diffused into the catalyst droplets until a saturated concentration is reached, resulting in the formation of

SiNWs. From the results, it can be observed that formation of NWs at low rf power is low and the growth of NWs is suppressed at high rf power, thus resulting in the growth of ordered Si film. This is due to the higher presence of SiH_3 radicals at low rf power and stronger H etching effects at high rf power. Thus, growth of ordered Si film limits the catalyst activity for SiNWs growth. Therefore, the decrease in the formation of SiNWs at low rf power and suppression of SiNW growth at high rf power of 100 W explain the growth kinetics of SiNWs by this technique.

4.3.2 Energy dispersive X-ray analysis

Figure 4.10 shows the EDX spectra of the droplets capped SiNWs prepared on ITO-coated glass by simultaneous Au evaporation and H_2 diluted SiH_4 gases decomposition using hot-wire assisted PECVD. Two droplet-capped SiNWs, namely nanowires 1 and 2 were examined. For nanowire 1, both the EDX spectra taken on catalyst droplet and NWs stem show the signals of Si, Au, In, Sn and O. The elemental compositions of the catalyst droplet and the stem of nanowire 2 are similar to the nanowire 1, except the absence of Au element. It is interesting to note that not all the catalyst droplets examined by EDX show the presence of the Au element. In fact, for both nanowires 1 and 2, the difference between the EDX spectra taken on the catalyst droplets and NWs stems is the higher In signal observed within the catalyst droplet which is significantly low in the stem of the NWs. This indicates the In islands sputtered out from the ITO layer by H_2 plasma treatment can act as a catalyst alone without the assistance of the Au element to induce the growth of SiNWs.

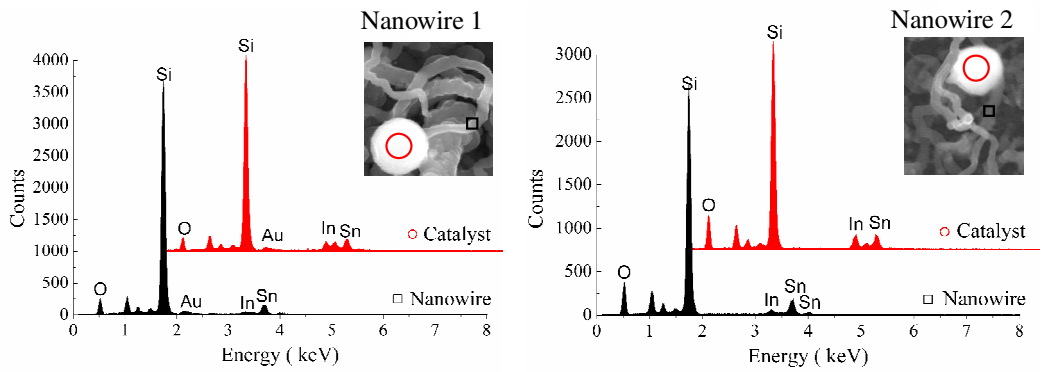

Figure 4.10: EDX spectra taken on the catalyst droplets and NW stems of the droplet capped SiNWs.

4.3.3 Micro-Raman analysis

4.3.3 a) Optimization of excitation laser power for Raman measurements

As reported by researchers (*Piscanec et al. 2003; Scheel et al. 2006*), SiNWs are very sensitive to the laser power of the Raman measurement. Operating Raman with high laser power could cause localized heating on the samples and give rise to the shifting in the peak position of transverse optical (TO) phonon mode (*Piscanec et al. 2003; Scheel et al. 2006*). Therefore it is important to optimize the scanning laser power before measuring the Raman signal. Figure 4.11 shows the Raman spectra of SiNWs samples prepared on ITO glass substrate scanned at laser power variy from 1.5 to 20 mW. Noticeably, increase in laser power leads to a shift in the Raman peak towards low frequency and a broadening of the peak width. For laser power ≤ 10 mW, the Raman peak is slightly shifted from 508.0 cm^{-1} (lowest laser power) to 504.8 cm^{-1}, while significantly shifted to 493.6 cm^{-1} and 488.2 cm^{-1} with increase in the applied laser power to 15 and 20 mW, respectively. Moreover, the Raman peak shape transforms from asymmetrical at lower frequency to symmetrical in shape for laser power > 10 mW. This causes a loss in the real structural information for the SiNWs samples. While, for the case with too low laser power (< 1.5 mW), the Raman signal becomes noisy, resulting in a decrease in signal to noise ratio, therefore results in loss in the information

due to insufficient signal detected. Thus, in the following work, a laser power of 1.5 mW is applied to the Raman measurements of SiNWs samples.

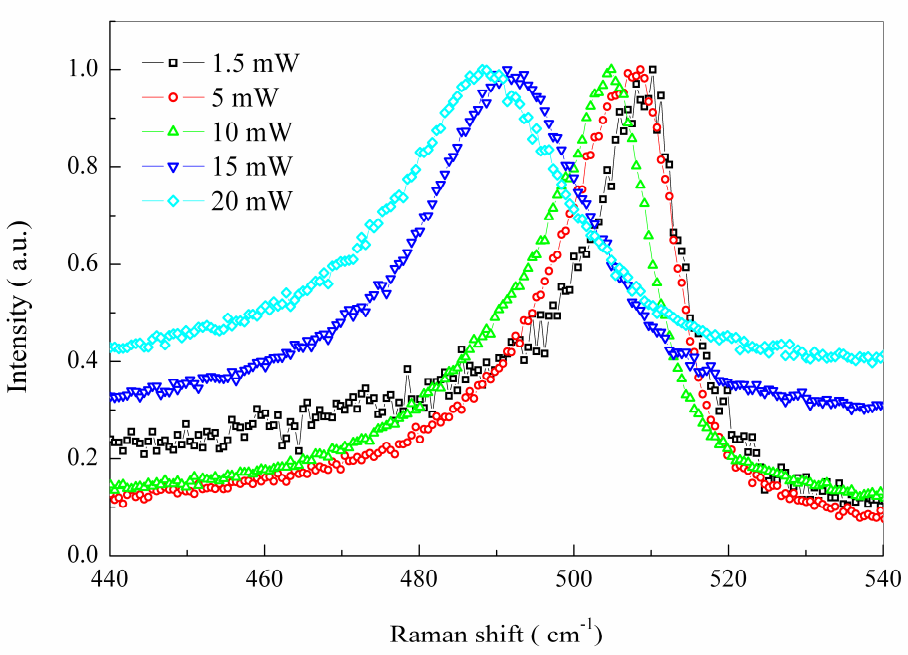

Figure 4.11: Raman spectra of the SiNWs samples scanned at different laser power.

4.3.3 b) Effect of rf power on Raman spectra

Figure 4.12 shows the Raman spectra for SiNWs and microstructures prepared on the ITO glass at different rf powers. The sample prepared at rf power of 20 W reveals a broad shoulder at ~480 cm^{-1} and a sharp peak at ~510 cm^{-1} corresponding to the amorphous and crystalline structures, respectively, within the sample. Increase in rf power to 40 W enhances the crystalline Si peak and suppresses the amorphous broadening. Further increase in rf power leads to the suppression in crystalline peak in Raman spectra. This indicates a tendency of amorphous Si structures formation at higher rf power deposition. A typical Lorentzian deconvolution of the TO phonon mode into 3 related peaks corresponding to the crystalline, intermediate or grain boundary and amorphous components of Si is inserted in Figure 4.11. The crystalline volume fraction, X_C (in %) of the samples can be calculated from relation 3.4. The crystallite size, D_R for samples prepared at different rf power was estimated from the shift in Raman crystalline

Si peak from the relation 3.3. The X_C and D_R of the samples prepared on the ITO glass at different rf power are presented in Table 4.1.

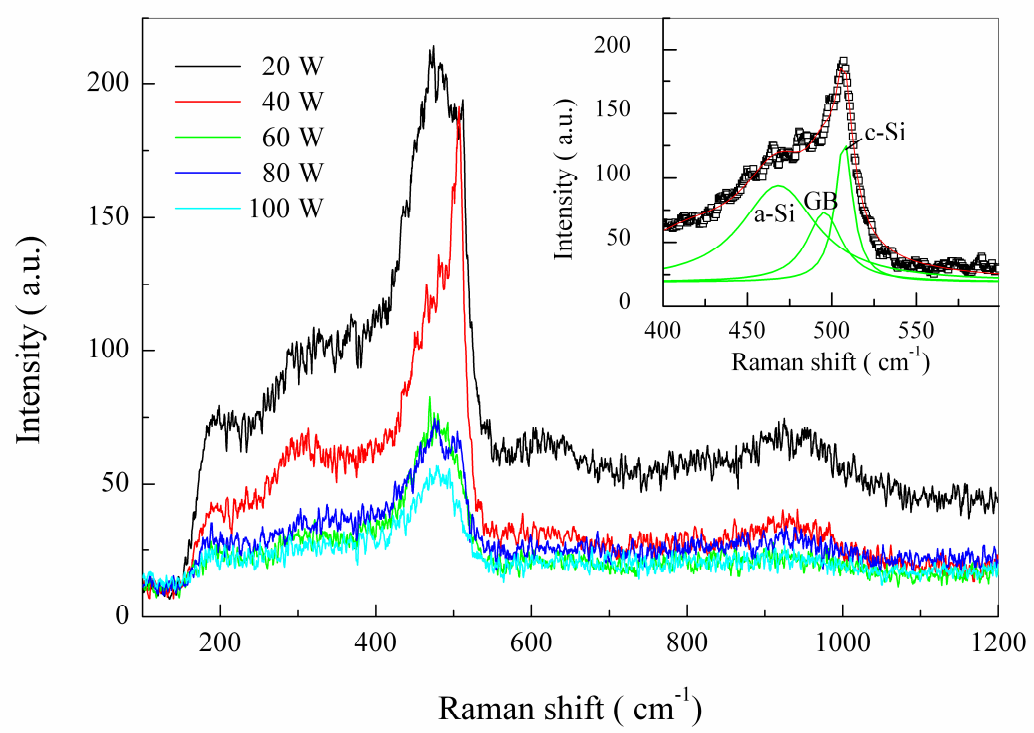

Figure 4.12: Raman spectra of the SiNWs and microstructures prepared at different rf power. The inset shows a typical deconvolution of the TO phonon mode of Si into amorphous, grain boundary and crystalline components.

4.3.3 c) Crystalline volume fraction and crystallite sizes

Generally, the X_C and D_R of samples are decreased with increase in rf power. The X_C is highest at rf power of 40 W, and is significantly reduced to below 20% at higher rf power. Meanwhile, D_R of the samples is reduced from ~3.4 to ~1.6 nm with increasing in rf power from 20 to 100 W. This indicates formation of Si nanocrystallites within the samples. Si nanocrystallites can be formed on the SiO_x/Si interface of SiNWs (*Sivakov et al. 2010*) or through the radial deposition of the uncatalyzed SiH_x species (*Adachi et al. 2010*). Since the Raman signals were taken within a scanning area of 2 – 7 μm, which could cover the NWs and films structures within the samples, the obtained Raman spectra could be a mixture of signals for the NWs and background films. To differentiate it, Raman mapping was carried out.

Table 4.1: Variation of X_C and D_R of the samples prepared on ITO glass substrate with rf power.

rf power (W)	X_C **(± 6%)**	D_R **(± 0.1 nm)**
20	39	3.4
40	46	2.9
60	10	2.4
80	15	2.5
100	-	1.6

4.3.3 d) Raman mapping

FESEM image and Raman imaging features of the SiNWs synthesized at rf power of 80 W are illustrated in Figure 4.13 (a) and (b), respectively. From the FESEM image, the sample actually consists of a mixture of SiNWs and Si nanoparticles (SiNPs). The Raman image illustrates the distribution of the SiNWs (red) and the SiNPs (green) over the sample. Raman spectra obtained from the SiNWs and SiNPs region are shown in Figure 4.13 (c). The Raman signal of the SiNWs was separated from the background of deposited Si films. It shows higher crystalline structures of SiNWs compared to the amorphous like structures for uncatalyzed SiNPs below the NWs. Thus, the actual crystallite size of Si within the SiNWs prepared at rf power of 80 W, was calculated from Raman peak using relation 4.4 is 2.9 ± 0.1 nm.

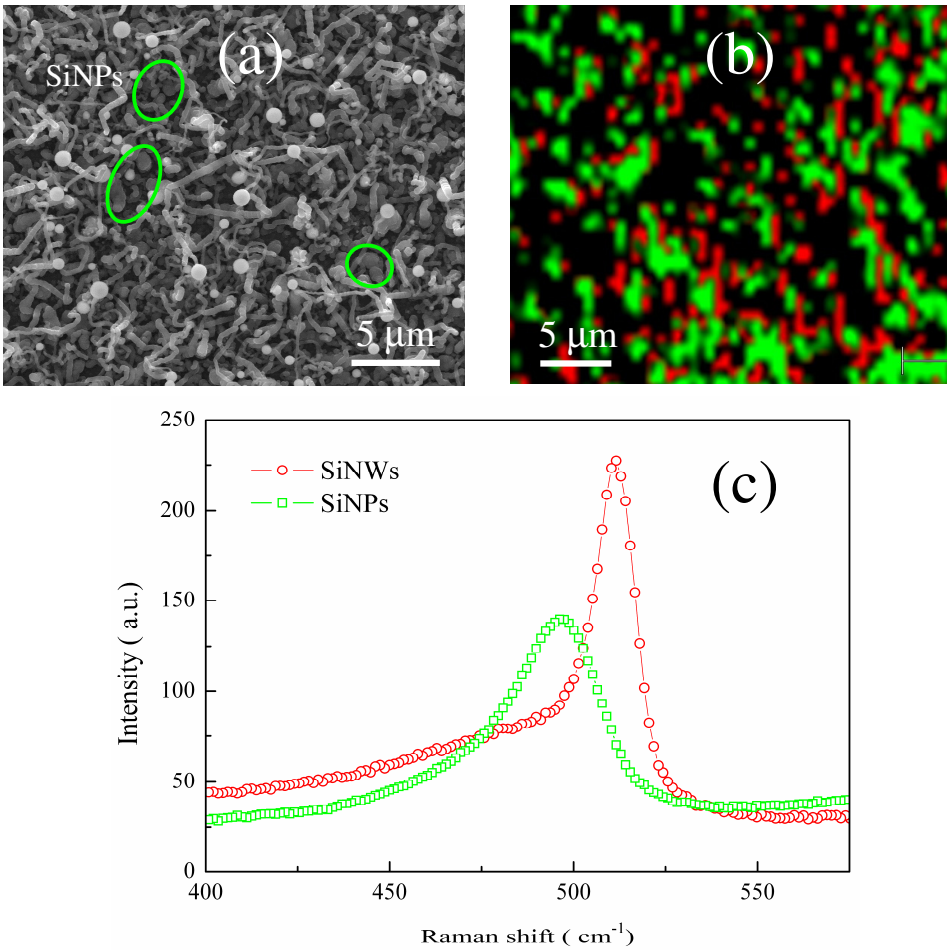

Figure 4.13: (a) FESEM image, (b) Raman mapping features of the SiNWs synthesized at rf power of 80 W, and (c) Raman spectra from the green and red region of the sample.

4.3.4 Structural studies on single nanowire

4.3.4 a) Selected angle electron diffraction

The crystallinity of the SiNWs prepared at different rf powers is examined using SAED patterns and HRTEM micrographs. Figure 4.14 (a) shows a typical TEM micrograph of our as-grown SiNWs. SAED patterns taken on the SiNWs prepared at rf power of 40, 60 and 80 W are depicted in Figures 4.14 (a), (b) and (c), respectively. It clearly shows that the diffraction pattern transform from discrete bright spots into weaker spots, and the amorphous ring are apparent with increase in rf power. The discrete electron diffraction spots of crystal Si indicate a highly crystalline structure of NWs prepared at rf power of 40 W. In agreement with the Raman spectra, the crystallinity of the SiNWs

is decreased with increase in rf power. Furthermore, the weak background spotty crystalline diffractions and amorphous background observed in diffraction patterns of SiNWs prepared at higher rf power suggest the existance of Si nanocrystallites within SiNWs.

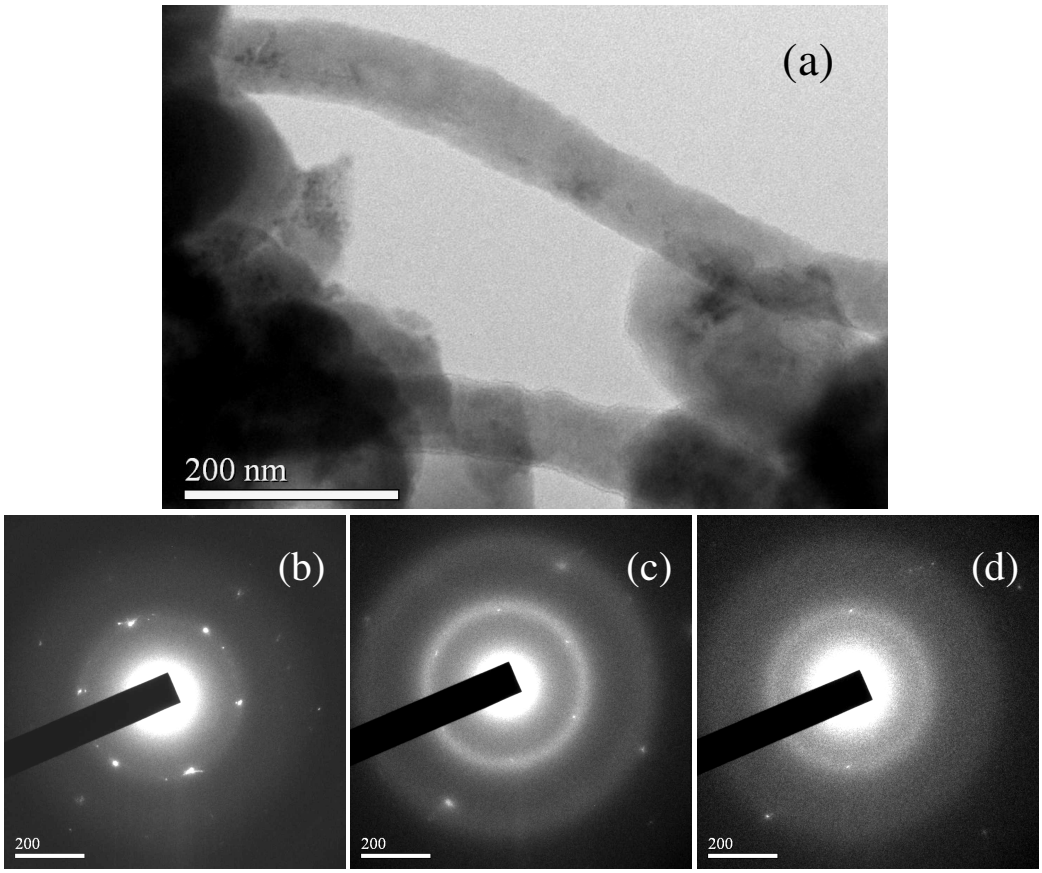

Figure 4.14: (a) typical TEM micrograph of the SiNWs. SAED patterns of the SiNWs prepared at rf power (b) 40, (c) 60, and (d) 80 W.

4.3.4 b) High resolution transmission electron microscopy

Figure 4.15 (a) shows the TEM image of SiNWs prepared at rf power of 40 W. The NWs exhibit a rough surface and are covered by a thin layer of SiO_x shell with thickness of ~2-3 nm. The HRTEM image of the SiNWs illustrated in Figure 4.15 (b) reveals long range of crystalline structures within the NWs. The lattice spacing is about 0.31 nm which corresponds to Si(111) crystalline orientation plane consistent with the XRD results in Figure 4.7. From Figure 4.15 (c), the twinning defect can be observed in

lateral side of the NWs, which causes a dislocation in the crystal lattice. Note, lateral twining defect is usually formed in the In induced SiNWs (*Conesa-Boj et al. 2010*).

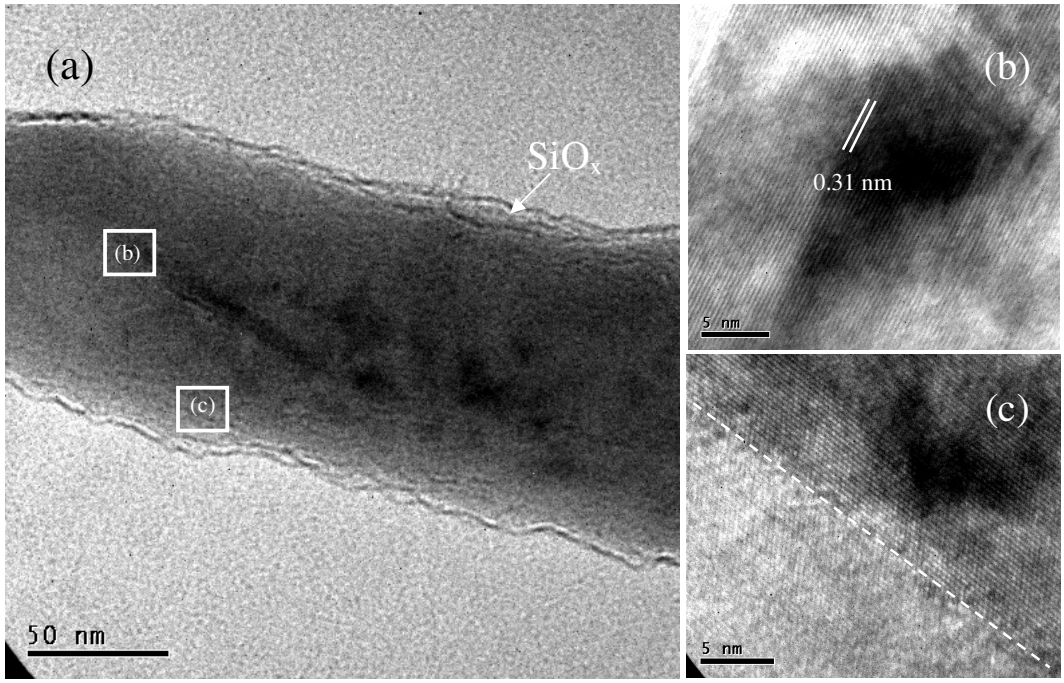

Figure 4.15: (a) TEM and (b,c) HRTEM micrographs of the SiNWs synthesized at rf power of 40 W.

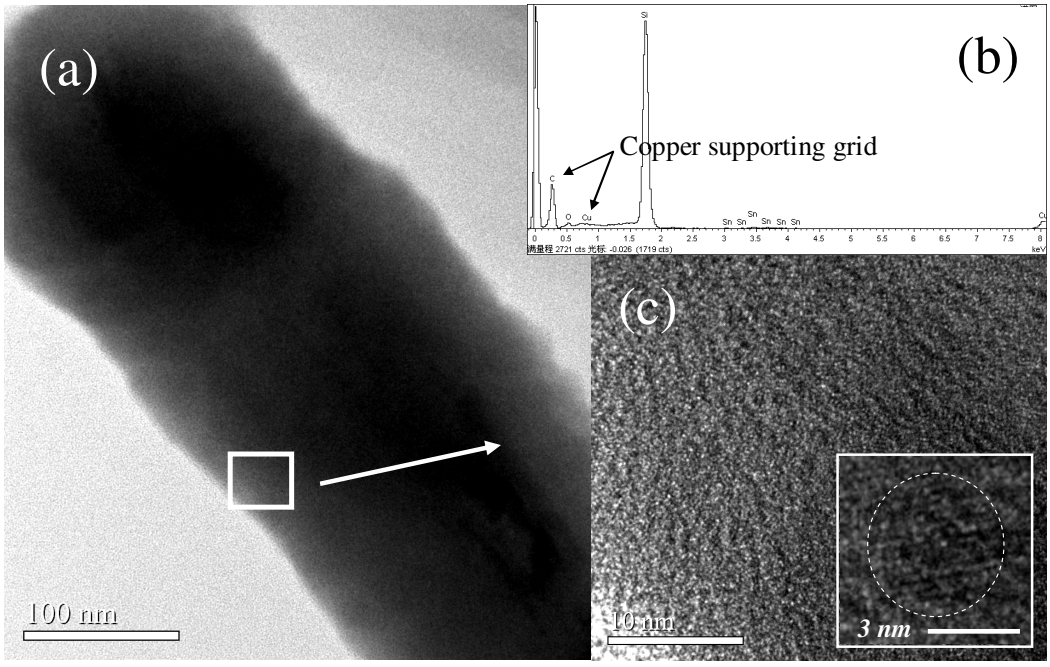

Figure 4.16: (a) TEM and (c) HRTEM micrographs of the SiNWs synthesized at rf power of 80 W. (b) EDX spectrum taken on the NWs. The HRTEM micrograph of Si nanocrystallite with crystallite size ~3 nm is inserted in (c).

From TEM micrograph of the SiNWs prepared at rf power of 80 W [Figure 4.16 (a)], the SiO_x shells are unremarkable compared to the SiNW prepared at 40 W, while the surface of NWs is covered by an amorphous structure. The EDX analysis [Figure 4.16 (b)] on the NWs showed weak oxygen content of 1.3 wt%, thus, confirming the passivation of amorphous Si layer on the NWs. The amorphous Si layer covering the NWs is believed to be due to radially deposited uncatalyzed SiH_x species on the surface of the NWs via vapor-solid process. The HRTEM image reveals the large amount of Si nanocrystallites embedded within the amorphous matrix in the NWs. Obviously, increase in rf power to 80 W causes a decrease in crystallinity, leading to the formation of Si nanocrystallites within the SiNWs. Inheriting the crystal orientation of SiNWs, the nanocrystallites show preferred in Si(111) crystallographic orientation. The sizes of Si nanocrystallites estimated from the HRTEM micrographs vary from 1 to 4 nm with an average size of 2.8 ± 0.7 nm, which is close to the calculation from the Raman spectrum (2.9 ± 0.1 nm).

4.4 GROWTH MECHANISMS

4.4.1 Au-catalyzed and In/Au-catalyzed growth of Si nanowires

Figure 4.17 illustrates the growth mechanisms of the Au-catalyzed and In/Au-catalyzed SiNWs by using this technique. Commonly, the SiNWs showed catalyst droplets capping the top of the NWs, indicating that the VLS process contributes to the growth. For the Au-catalyzed growth of SiNWs [Figure 4.17 (a)], the Au islands formed eutectic with Si atoms in the substrate, which then melted at substrate temperature above eutectic temperature of Au/Si (~370^{o}C). The Au/Si islands then aggregate with each other to form larger size of Au/Si droplets. The SiH_4 and H_2 source gases introduced into the reactor are dissociated into Si and SiH_x ionic species when rf power is applied to the powered electrode. Continuous feeding of the Si and SiH_x species into the Au/Si alloy droplets saturates the droplets until supersaturation of the Si atoms is reached in the Au/Si droplets. The supersaturated Si atoms in Au/Si droplets then undergo phase separation, resulting in the protrusion of the Si atoms from the Au/Si droplets, thus forming NWs. The Au-catalytically-grown NWs normally are capped by smaller size of metal droplets as the contact angle of Au/Si droplet on substrate is only about 43 ° (*Ressel et al. 2003*). For the In/Au-catalyzed growth NWs [Figure 4.16 (b)], the In atoms sputtered out from the ITO layer by H_2 plasma treatment combine with the Au droplets evaporated from the heated tungsten filament, forming In/Au alloy catalyst to induce the growth of SiNWs. The In detached from the ITO layer is believed to form droplets on the substrate due to the high substrate temperature of 400^{o}C which is higher than the melting point of In (156.6^{o}C). The droplets produce a contact angle of about ~125 ^{o} with the substrate (*Mattila et al. 2006; Nagai et al. 1998*). The large contact angle reduces the contact area between In/Au droplets and substrate. The Si and SiH_x species diffuse into the In/Au droplets, converge and saturate at the interface of the droplets and substrate. Phase separation and precipitation of Si atoms occurs to form

SiNWs below the In/Au droplets. The SiNWs formed from In/Au-catalytic growth have large catalyst droplets capping them as a result of this.

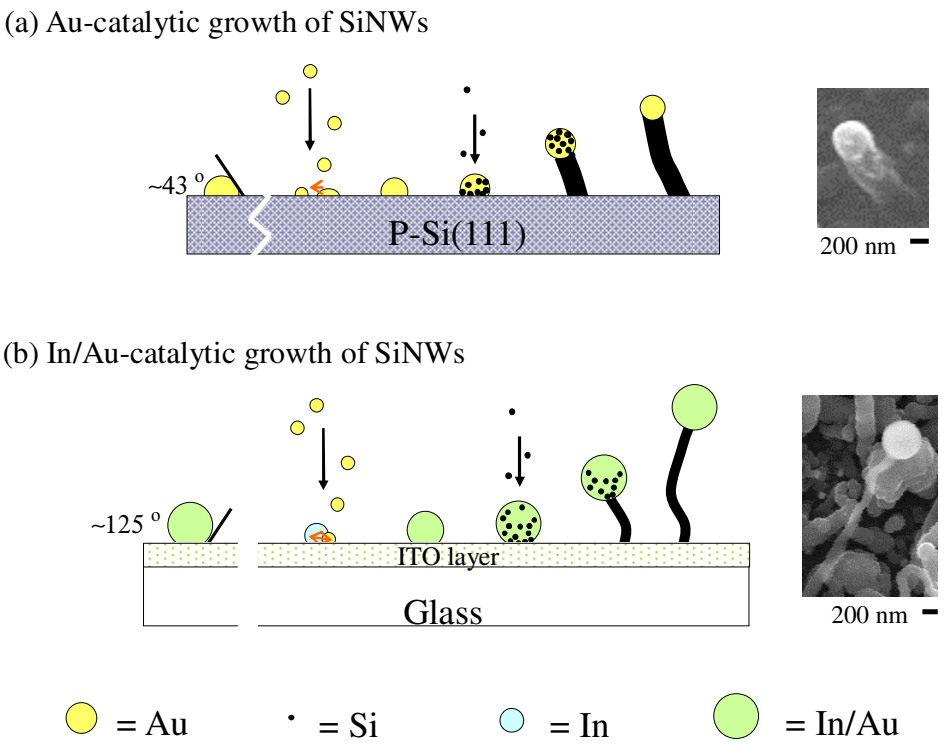

Figure 4.17: The proposed growth mechanism of (a) Au-catalyzed and (b) In/Au-catalyzed growth of SiNWs on p-Si(111) and ITO-coated glass substrates, respectively, using PECVD technique.

4.4.2 Effect of rf power on Si nanowires grown by simultaneous Au evaporation and source gas decomposition

The growth mechanism of the SiNWs grown by simultaneous evaporation of Au and dissociation of SiH_4 and H_2 gases in HW-PECVD generally follow the In/Au-catalyzed growth mechanism as presented in Figure 4.17 (b) of Section 4.4.1. The difference between these mechanisms is the incorporation of Au into the In catalyst droplet capping the NWs. Au elements are not observed in some of the catalyst droplets capping the NWs deposited by simultaneous evaporation of Au and dissociation of precursor gases [refer to Figure 4.10 (a)]. This could be due to the precipitation of Si in the In droplets prior to Au evaporation, therefore, some of the evaporated Au droplets did not

combine with the In droplets on the substrate, as illustrated in Figure 4.18 (a). This suggests that the SiNWs can actually be induced by In catalyst alone without the assistance of Au elements. Further deposition carried out by dissociation of SiH_4 and H_2 gas using PECVD on H_2 plasma-treated ITO-coated glass substrate (not shown here) shows similar morphology for the SiNWs.

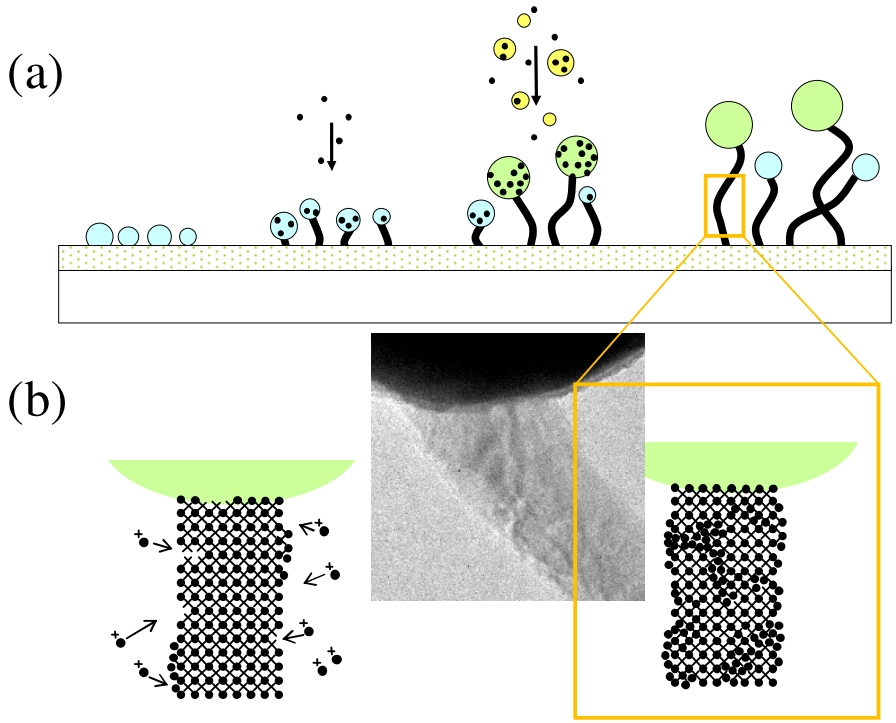

Figure 4.18: (a) Growth mechanism of the In/Au-catalyzed SiNWs by simultaneous Au evaporation and SiH_4 and H_2 gases dissociation. (b) Effect of rf power on the morphology and structural characteristic of SiNWs.

The applied rf power strongly influences the morphology and structures of the SiNWs. Increase in the applied rf power shows two significant effects on the NWs formed, namely the increase in diameters and decrease in crystallinity of the SiNWs. As discussed in Section 4.3.1.3, the uncatalyzed SiH_x species reaching the substrate tend to deposit onto the surface of the NWs. This roughens the surface of the SiNWs. Increase in rf power increases the rate of SiH_4 dissociation, thus increasing the amount of uncatalyzed SiH_x species. This eventually increases the rate of the sidewall deposition on the NWs. However, the increase in rf power is also accompanied by the enhancement

in ion bombardment, which can affect the structures of the NWs and sidewall deposited Si layer. The excessive ion bombardment destroys the crystalline structures of the SiNWs, resulting in the formation of amorphous and nanocrystalline structures within the NWs, as presented by the SiNWs synthesized at rf power of 60 and 80 W. The sidewall deposited Si layer also shows amorphous structures, contributed by the bombardment of uncatalyzed ionic species.

4.5 SUMMARY

Randomly oriented SiNWs were synthesized by combining Au wire evaporation using hot filament and dissociation of H_2 diluted SiH_4 using rf plasma discharge on c-Si and ITO-coated glass substrates. The In/Au induced SiNWs were longer (several microns) compared to the Au induced SiNWs, which indicated a higher catalytic ability of the In/Au catalyst in low temperature growth of SiNWs. In/Au-catalyzed SiNWs revealed significantly large catalyst size to NWs diameter ratio, $r_{c\text{-}nw}$ ~4.1 compared to the pristine Au-catalyzed SiNWs with $r_{c\text{-}nw}$ ~1.2 due to the wettability nature and low melting point of In. Similar morphology of In/Au-catalyzed SiNWs were obtained through simultaneous evaporation of Au wire and dissociation of H_2 diluted SiH_4 using HW-PECVD. Increase in rf power increased the density of the NWs, however, the growth of SiNWs was totally suppressed at rf power of 100 W (power density of ~1273 $mWcm^{-2}$) due to deactivation of catalyst effect. The SiNWs grew at lower rf power ($\leq$ 40 W) exhibit higher crystallinity, while, the crystallite size and crystallinity are reduced for SiNWs synthesized at higher rf power. This results in the formation of nanocrystalline structures embedded within an amorphous matrix of SiNWs at rf power of 60 and 80 W.